An experimental investigation on wake mixing and steering techniques

Journal of Physics: Conference Series **3224** (2026) 032050 doi:10.1088/1742-6596/3224/3/032050

An experimental investigation on wake mixing and steering techniques

D Bortolin[1], S Tamaro[1], F Campagnolo[1], F V Mühle[1], M Manolesos[2], A Croce[3] and C L Bottasso[1]

[1]Wind Energy Institute, Technical University of Munich, 85748 Garching b. München, Germany

[2]School of Mechanical Engineering, National Technical University of Athens, Iroon Politechniou 9, 15780, Athens, Greece

[3]Department of Aerospace Science and Technology, Politecnico di Milano, Via La Masa, 34, 20156, Milano, Italy

E-mail: carlo.bottasso@tum.de

Abstract. Wake steering and wake mixing are two flow-control strategies aimed at improving wind-farm performance by redirecting turbine wakes or accelerating their recovery to increase downstream turbine and overall power production. Among wake-mixing approaches, the Helix and Dynamic Yaw techniques have recently attracted significant attention. Although both strategies have shown promising results in previous studies, they have rarely been compared directly. This experimental work evaluates the performance of wake steering and mixing, relative to the conventional greedy operation, within an extended three-turbine cluster tested in a large boundary-layer wind tunnel. The analysis considers both power production and the resulting damage equivalent loads across different wind directions. Several combinations of wake steering and wake mixing are explored to identify potential synergies. In terms of power production, the results show that an optimally implemented wake-steering strategy outperforms wake mixing. The actuated turbine experiences higher loads when wake mixing is applied, while the load trends on the downstream turbines generally mirror their corresponding power trends.

1. Introduction

Wake steering has been widely demonstrated as an effective strategy to increase power production at the wind-farm level [1, 2]. More recently, wake mixing has also shown strong potential for enhancing farm performance, even outperforming wake steering in certain scenarios [3]. Wake mixing relies on actively exciting the wake downstream of a turbine to accelerate its recovery and boost the power production of downstream machines. Two approaches that have been extensively studied are the "Helix" and Dynamic Yaw (DY). The Helix strategy [4] relies on cyclic pitch oscillations of the blades. This cyclic pitching generates a rotor-in-plane moment that rotates in time and introduces a helical pattern in the wake, thereby accelerating its recovery [5]. DY [6], on the other hand, is implemented by imposing a periodic motion of the nacelle yaw angle around its mean position [7]. These oscillations result in a promoted lateral meandering of the wake, which in turn accelerates its recovery.

The present experimental study provides for a comprehensive investigation of active wake mixing and wake steering, as well as their combined application for different wind directions.

We study a cluster of three turbines, extending the current state of the art beyond the one- and two-turbine configurations considered by most prior work on this topic.

The paper is structured as follows: the experimental setup is first described, followed by an analysis aimed at identifying the optimal power setpoints for the different control strategies. Helix, DY, and wake steering are compared for different wind direction angles $\psi = [-2° : 1° : 2°]$, where $\psi = 0$ corresponds to full waking of the three aligned wind turbines. For wake steering, two scenarios are considered: one in which both upstream rotors are yawed, and another in which only the most upstream one is misaligned. This narrow range of wind directions is found to be sufficient to evaluate the extent to which wake mixing outperforms wake steering. Furthermore, the combined effect of wake steering and wake mixing is also investigated. First, the upstream turbine is actuated using simultaneous wake mixing and different yaw angles. Subsequently, the combination of wake mixing on the first turbine and wake steering on the second is also tested. Finally, cluster-level fatigue results are evaluated and compared across different wind directions, providing insight into the impact of wind farm control on the structural loading through the analysis of Damage Equivalent Loads (DELs). A final discussion compares the behaviour of the Helix approach observed in this study with findings from existing literature. In particular, we highlight the key differences and similarities between the turbine model used in this work and those examined in previous numerical and experimental works.

2. Experimental setup

A cluster of three scaled wind turbine models G1 [8] was installed on a 13 m diameter turntable in the boundary-layer test section of the Politecnico di Milano wind tunnel [9]. In this set of experiments, the turntable was used to simulate different wind directions ψ with an accuracy of $\pm 0.1°$. Figure 1 shows a representation of the measurement setup.

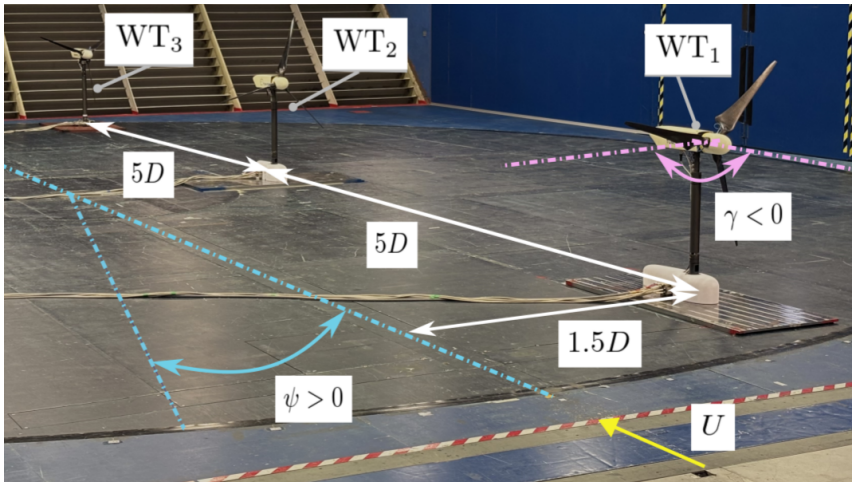

Figure 1. Experimental setup showing the three model turbines mounted on the wind tunnel turntable. The picture includes the reference convention for nacelle yaw angle and wind direction.

The scaled wind turbine models have a rotor diameter $D = 1.1$ m, are labelled WT_1, WT_2, and WT_3 moving downstream and are separated by a distance equal to $5D$. The yaw system described in [10] was installed to increase the yaw rate of the G1, thereby extending the range of DY amplitudes and frequencies to test.

All experiments were carried out under inflow conditions characterised by a turbulence intensity TI = 6% at hub height, a power-law shear exponent $\alpha = 0.14$, and an integral turbulence

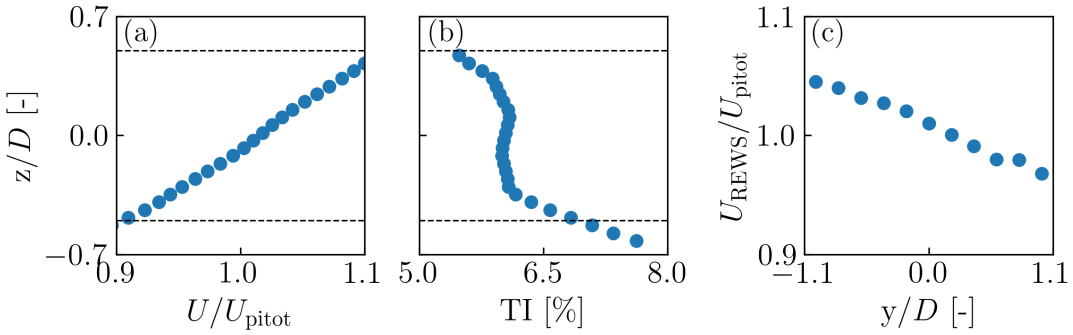

Figure 2. Wind tunnel inflow characteristics: vertical streamwise velocity (*a*) and turbulence intensity (*b*) profiles, and lateral streamwise velocity profile (*c*). In (*a*) and (*c*), U and U_{REWS} are normalised with respect to the pitot tube velocity U_{pitot}. The top and bottom points of the rotor are indicated with dashed black lines. Hub height is located at (y,z) = (0, 0).

length scale $0.79D$. The vertical turbulence intensity profile is shown in 2(b). The vertical and lateral wind-speed profiles are shown in figure 2(a) and figure 2(c), respectively. The lateral streamwise wind velocity is shown by normalising the rotor-equivalent wind speed experienced by the rotor (U_{REWS}), as it is moved laterally, with U_{pitot}. The vertical streamwise velocity profile, instead, is obtained by scanning a vertical line $4D$ upwind of WT_1 with a three-component constant-temperature hot-wire probe. During the experiments, the ambient wind speed U_{pitot} was measured using a Pitot tube mounted at hub height, positioned $4D$ upstream of WT_1. The scaled wind turbines were controlled by a dedicated real-time Bachmann M1 system, which provides setpoints for torque, pitch, and yaw. The control system simultaneously acquires torque, shaft bending moments, and rotor azimuth at a sampling rate of 2.5 kHz. All other measurements, such as tower-base bending moments, are recorded at a sampling rate of 250 Hz. Each experimental data point presented in this work corresponds to the temporal average of one minute.

For all experiments, the inflow wind speed U_{pitot} was set to approximately 5.5 m/s, corresponding to a turbine operation below rated conditions. In this and in the following sections, baseline or greedy control refers to the use of a variable speed $k\omega^2$ torque controller [11] for all three machines, where ω is the rotor speed. During greedy operations, the rated rotor speed is 850 RPM, and the turbines operate at a power coefficient $C_P \approx 0.41$ and a thrust coefficient $C_T \approx 0.81$.

3. Identification of the optimal operating points

In the first set of experiments, the optimal power setpoints for both DY and Helix were determined under fully aligned inflow conditions.

3.1. Dynamic yaw

For the DY strategy, the nacelle yaw angle γ was driven with a sinusoidal motion defined as $\gamma(t) = A_{\text{DY}} \cos(2\pi f_{\text{DY}} t)$, with A_{DY} and f_{DY} being the DY amplitude and frequency of oscillation, respectively.

Figure 3 shows the normalized power of the wind farm $p_{n,WF} = \sum_i p_{ni}$ with respect to the greedy control, where $p_{ni} = p_i/(\frac{1}{2}\rho A U_{\text{pitot}}^3)$. p_i, with $i = [1, 2, 3]$, is the power produced by WT_1,WT_2 and WT_3, respectively, ρ the flow density and A the swept area of the rotor. Both the amplitude A_{DY} and non-dimensional frequency $\text{St} = f_{\text{DY}} D/U_{\text{pitot}}$ were systematically

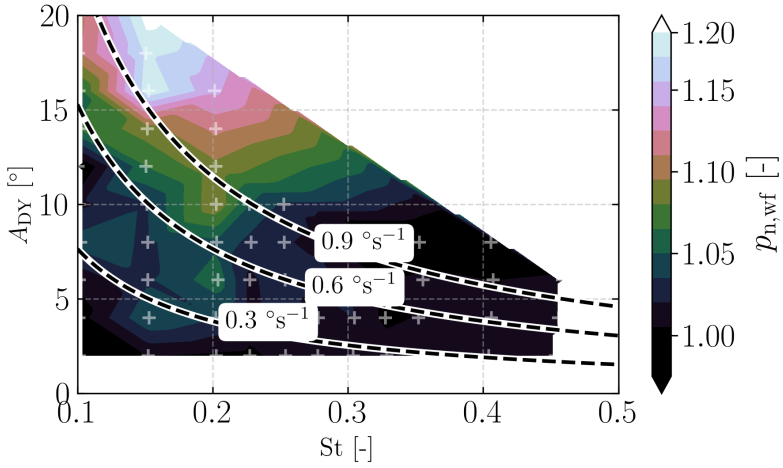

Figure 3. Cluster power normalised with a baseline case $p_{n,\mathrm{WF}}$ plotted against amplitude and Strouhal number of actuation for dynamic yaw for $\psi = 0°$. The black dashed lines represent full-scale equivalent yaw rates. The white crosses in the background mark the locations of the measurement points.

varied in order to identify the most effective operating conditions. The white regions in the figure correspond to operating conditions that were not tested due to yaw rate limitations of the scaled model.

The optimal operating point was selected as a trade-off between realistic full-scale yaw rate constraints and performance. In general, higher yaw rates for DY are associated with increased power gains. In this study, the yaw rate was fixed to a realistic value of 0.6°/s, and the operating point corresponding to the maximum total cluster power was selected for the analysis. The setpoint features an amplitude of 12° and a Strouhal number of approximately $St \approx 0.125$. The wind farm power increase with these DY settings is approximately +7.6%. DY has the potential to deliver power gains up to +20%, well above the value selected here. Consequently, the power setpoints adopted in this study should be considered a conservative lower bound on the improvements that DY can achieve. As full-scale turbine technology continues to advance, the potential of DY may be further unlocked.

3.2. The Helix

The same approach used for DY was adopted for the Helix, for which the individual blade pitch varies as $\beta_i(t) = A_{\mathrm{Helix}} \sin(2\pi f_\beta t + \Phi_i)$ where A_{Helix} is the Helix amplitude, f_β the Helix pitch actuation frequency and $\Phi = [0, 2/3\pi, 4/3\pi]$ the phase difference between the actuation of the three blades. If the Helix pitch actuation frequency f_β is lower than the rotor rotational frequency f_r, the resulting in-plane moment generates a wake that rotates in the clockwise (CW) direction (for an observer that looks downstream). Conversely, when f_β exceeds the rotational frequency, the wake rotates counterclockwise (CCW). The Strouhal number for the Helix actuation is here defined as $\mathrm{St} = (f_\beta - f_r)D/U_{\mathrm{pitot}}$. In this formulation, a negative Strouhal number identifies the CW case, while a positive Strouhal number corresponds to the CCW case.

In agreement with [12], increasing the amplitude A_{Helix} generally led to higher power gains. In the present study, an amplitude $A_{\mathrm{Helix}} = 3°$ was selected. It is worth noting that the power gains produced by the Helix actuation do not stop at WT_2, but continue to propagate

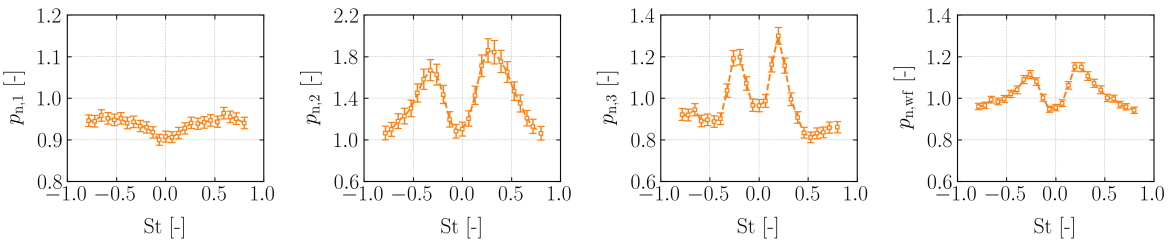

Figure 4. Local and cluster power normalised with a baseline case for $\psi = 0°$. The first wind turbine WT_1 performs mixing by Helix with an amplitude $A_{Helix} = 3°$ and a range of actuation frequencies. The other wind turbines located downstream are aligned with the inflow and operate in greedy power control mode.

downstream to the third turbine. The CCW case exhibits the highest power gain between the two Helix implementations and produces larger gains on both WT_2 and WT_3. The CW Helix also increases the power of both downstream turbines, resulting in a total cluster power gain of +11.3%. Since the objective of the study is to compare the strategies under conditions of maximum achievable power gain, the CCW Helix, resulting in an improvement in power of +15.01%, at a Strouhal number of $St = 0.25$, was selected.

3.3. Wake steering

The optimal nacelle misalignment for steering on WT_1 was determined by varying the yaw angle γ_1 within the range (-30°:3°:-18°) for positive ψ and (30°:-3°:18°) for negative ψ. For the aligned inflow configuration, both positive and negative yaw angle variations were tested and compared. The optimal yaw angles that maximise power production for the same three-turbine configuration in the case of steering on WT_1 & WT_2 were previously identified in [13]. In this study, those optimal yaw setpoints are adopted to implement wake steering on the two upstream turbines. The optimal yaw angles for Steering on WT_1 and steering on WT_1 & WT_2 are reported in table 1.

Table 1. Yaw angles resulting from cluster power optimisation corresponding to the two wake steering strategies, reported for each of the turntable angles investigated.

	ψ	-2°	-1°	0°	1°	2°
Steering on WT_1	γ_1	30°	30°	-21°	-21°	-27°
Steering on WT_1 & WT_2	γ_1	30°	29°	-29°	-27°	-30°
	γ_2	21°	24°	-17°	-19°	-21°

Due to a slight lateral non-uniformity in the wind tunnel inflow – visible in figure 1(c) – the optimal yaw angles are not perfectly symmetric with respect to the aligned inflow condition. However, since in this study the turntable misalignment is limited to a maximum of 2°, the turbines experience wind-speed variations of no more than 1.5% relative to the Pitot-tube measurement.

4. Results

4.1. Power production

Next, the results in terms of power production are presented. First, wake mixing and wake steering are directly compared, then their combination is evaluated, and finally the results for the Helix are compared to similar studies reported in the literature.

4.1.1. Comparison of wake mixing and wake steering

The control strategies are now compared for different wind directions. Figure 5 presents the local and cluster power plotted against ψ for different wind farm control approaches.

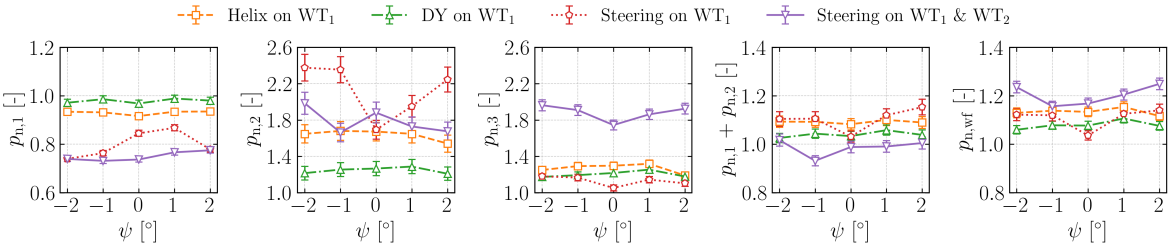

Figure 5. Local and cluster normalised power p_n with respect to a baseline case for a range of wind directions ψ. Values above 1 indicate an improvement with respect to greedy control. The first wind turbine WT_1 performs mixing by the Helix or DY, or it is misaligned by a yaw angle γ_1. Wake steering on both WT_1 and WT_2 is shown with a purple solid line.

Results indicate that both the Helix and DY yield power gains higher or comparable to the steering of the sole front wind turbine WT_1 (dashed red line in figure 5), but only under a rather limited wind inflow condition, in agreement with [3]. When $\psi \neq 0°$, the power gains of wake steering on $p_{n,2}$ increase significantly, whereas those of the wake mixing strategies tend to slightly decrease. Consequently, for non-perfectly aligned conditions, steering the first turbine achieves similar cluster-level power as the Helix and higher than DY. When steering is applied to both the first and second turbines (solid purple line in figure 5), the gains at the third turbine are significantly larger than those achieved with the use of the Helix or DY. The power losses observed on the upstream turbine with the Helix control are generally higher than those reported in literature; nevertheless, the relative power gains on the downstream turbine and on the whole cluster for the same helix amplitude appear to be higher, as discussed further in section 4.1.4.

4.1.2. Combination of wake mixing and wake steering on WT_1

Figure 6 reports the wind farm power under the combination of wake mixing and steering when $\psi = 0$. In these experiments, the upstream turbine is simultaneously yawed with different angles γ_1 and actuated with DY or Helix. When $\gamma_1 = 0°$, no steering is applied to the turbine; consequently, the rightmost points in figure 6 and 7 represent the sole baseline, Helix, and DY cases for the red, orange, and green curves, respectively.

The combined application of the two strategies does not yield a significant improvement compared to Helix or DY alone. As the upstream turbine inevitably suffers a substantial power loss when steered away from the wind, the downstream gains are insufficient to fully compensate for these losses, resulting in an overall net gain of not more than +2% with respect to the standalone wake mixing strategies. More specifically, the power losses on the upstream turbine scale proportionally with the yaw angle. In other words, the difference in power between the

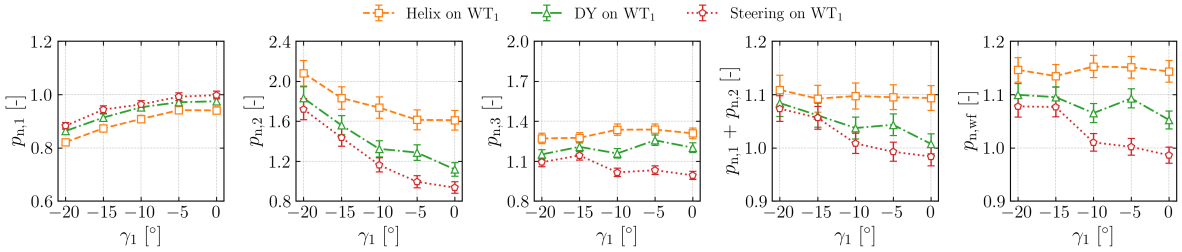

Figure 6. Local and cluster normalised power p_n with respect to a baseline case for a range of yaw angles. Values above 1 indicate an improvement with respect to greedy control. The first wind turbine WT_1 performs mixing by the Helix and DY, steering only the first turbine is represented with a red dotted line.

steering-only case and the Helix or DY strategies remains approximately constant as the yaw misalignment of WT_1 decreases. In contrast, the power gains observed on the second turbine do not follow the same trend. This is particularly evident for the Helix strategy: the power gain of the Helix relative to steering decreases noticeably as the yaw angle is reduced. For example, at zero yaw misalignment, the power gain of the Helix with respect to the red dashed curve on WT_2 is +61%, whereas at a yaw angle of $-20°$ the gain drops to just over half of that value, +36%. This combined behaviour of steering and mixing has a direct impact on the total power production of the cluster, resulting in an almost flat trend of cluster power across the investigated yaw angles.

4.1.3. Combination of wake mixing on WT_1 and wake steering on WT_2

Another set of experiments, in an aligned inflow condition, was conducted to assess whether steering the second turbine could enhance the cluster-level power gains when mixing is applied on WT_1. For this purpose, while WT_1 is actuated using either the Helix or DY strategy, WT_2 is yawed by an angle $\gamma_2 = (-24° : 3° : -12°)$. Figure 7 presents the results of these experiments.

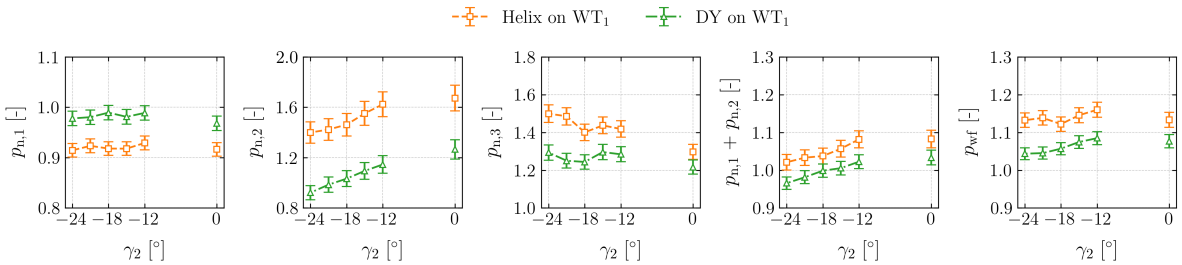

Figure 7. Local and cluster normalised power p_n with respect to a baseline case for a range of yaw angles. Values above 1 indicate an improvement with respect to greedy control. The first wind turbine WT_1 performs mixing by the Helix or DY, the second turbine WT_2 is yawed by an angle γ_2.

The power trends observed for WT_2 and WT_3 are similar for both the DY and Helix strategies. For WT_2, power decreases as the yaw angle is reduced, starting from the power setpoint corresponding to the respective wake-mixing configuration in which no yaw misalignment is applied to the second turbine. An opposite trend is observed for WT_3. As the wake of WT_2

is increasingly deflected away from the downstream turbine, the power production of WT_3 increases. The power increase scales with the yaw misalignment and shows a similar trend for both wake-mixing strategies. The reference level is the power gain achieved by each wake-mixing strategy when no yaw misalignment is applied to the second turbine. Results indicate that the additional power gained on WT_3 is always insufficient to compensate for the losses incurred on WT_2. Hence, similarly to the previous combination of steering and mixing, this approach does not lead to a substantial improvement in total cluster power. The same approach, although not shown here, was also tested for wind directions $\psi = 1°$ and $\psi = -1°$, yielding similarly negligible power improvements.

4.1.4. Comparison of the Helix with the state-of-the-art

Figure 8 shows the power of WT_1, WT_2, and WT_3, along with the cluster power considering two or three rotors, and compares them with numerical and experimental findings from the literature.

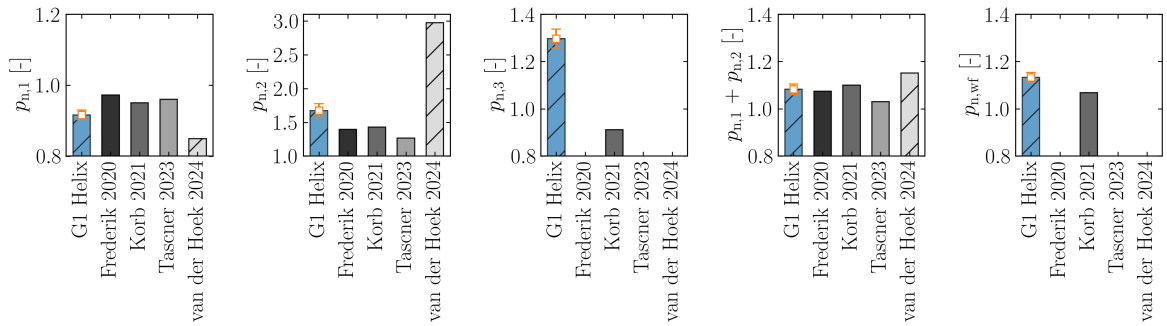

Figure 8. Local and cluster power under Helix actuation, normalised by the respective baseline cases, for the studies in [4], [14], [12], and [15]. Experimental results are shown with hatched bars, while numerical results are shown with solid bars.

The comparison includes three numerical studies (Frederik 2020 [4], Korb 2021 [14], Taschner 2023 [12]) and one experimental study (van der Hoek 2024 [15]). These works were selected to enable a fair comparison among the different results: despite some differences in the inflow conditions, all turbines were actuated using the optimal Strouhal number, and the turbine spacing was consistently set to 5D across all studies. Only in [14] were results for a third turbine reported, and the Helix approach was applied to the first two turbines in the row. In all the other studies, a two-turbine setup was considered. The power losses on the actuated turbine are higher in both experimental studies than in the numerical studies of full-scale machines, possibly due to unsteady aerodynamic effects. In contrast, the power gains observed on the second turbine are larger than those predicted numerically. Overall, however, the combined power gain of WT_1 and WT_2 for the G1 model aligns well with the numerical full-scale results, with values only slightly higher than those reported in [4] and [12].

4.2. Loads and fatigue

In this section, an analysis of the DELs is presented, using the signals acquired with strain gauges installed in the hub and in the tower base. The load assessments focus on the comparison between mixing and steering for different wind directions. Both tower and hub moments DELs – DEL_T and DEL_H respectively – were computed by projecting two measured orthogonal bending components onto the direction corresponding to the maximum DEL, and then normalising the

result by $1/2\rho\pi R^3 U_{\text{pitot}}^2$, where R is the rotor radius. Results, normalised with the greedy control case, are shown in figure 9.

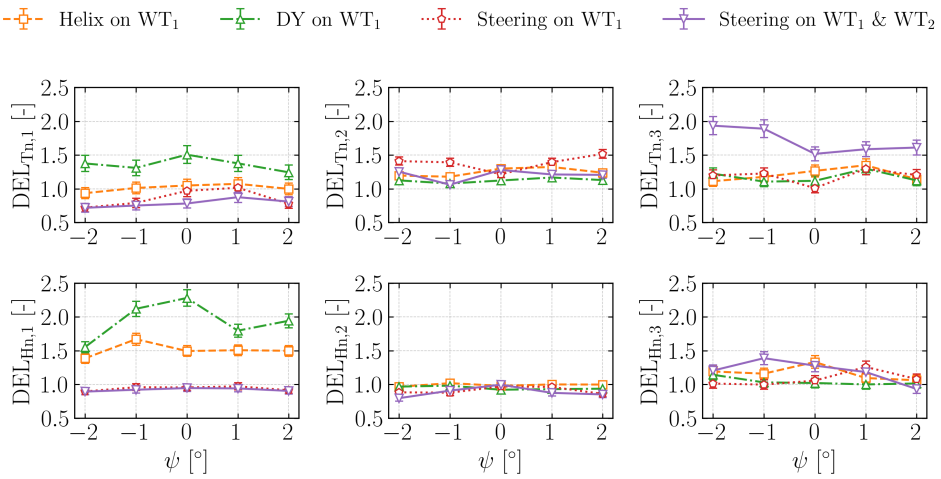

Figure 9. Local normalised $DEL_{n,i}$ with respect to a baseline case for a range of wind directions ψ. Values above 1 indicate an increase in damage with respect to greedy control. The first wind turbine WT$_1$ either performs mixing by the Helix and DY, or it is misaligned by a yaw angle γ_1. Wake steering on both WT$_1$ and WT$_2$ is shown with a purple solid line.

For all wind directions, the tower DELs of the first turbine show a slight reduction for both wake steering cases, consistent with the findings of [16]. For the Helix, the increase in tower DEL is negligible, whereas DY leads to a substantial rise of approximately +50%. The tower DELs of the second and third turbines follow the power trends closely, as expected. The hub DELs exhibit a different behaviour compared to the tower loads. The impact of wake steering on hub loads is negligible across all wind directions. In contrast, the Helix results in an increase of around +50%, and DY can have increases exceeding +100% for certain wind directions. For the second turbine, the influence on hub loads remains marginal, while for WT$_3$ an increase is observed, particularly in the Helix case and when steering is applied to both WT$_1$ and WT$_2$.

5. Summary and outlook

This work compared the effects of wake steering, wake mixing, and their combined application on both power and load performance under different wind directions in a three-turbine cluster.

For a two-turbine cluster, power results indicate a strong dependency of the effectiveness of wake mixing on ψ. Maximum performance is achieved under conditions of full rotor overlap, while effectiveness decreases with respect to steering as soon as the wind direction deviates from full rotor alignment, consistently with the numerical findings of [3]. In contrast, for a three-turbine cluster, results show that wake steering applied to the two most upstream rotors outperforms any wake mixing strategy involving only WT$_1$.

The power results from combining wake mixing and wake steering show no clear benefit. When wake mixing is active, and the turbine is simultaneously yawed, the response of the second machine suggests a mutual detrimental interaction between steering and the Helix. Further investigations are required to identify the physical mechanisms responsible for this behaviour.

Regarding the load results, WT1 experiences reduced or only slightly affected DELs when wake steering is applied. In contrast, both DY and Helix introduce a significant increase in hub loads on the actuated turbine. For the second and third turbines, the load trends generally follow the corresponding power trends. In the two-turbine cluster, wake mixing remains beneficial for power production under fully aligned conditions. However, the increased fatigue loads on the actuated turbine introduce a trade-off between power gains and structural loading. Evaluating this trade-off requires considering several factors, including market conditions, turbine lifetime, and environmental operating conditions. In this configuration, wake steering appears to be a more robust strategy for increasing power production while limiting additional structural damage to the turbine.

This study is limited to static and fixed wind direction variations; future investigations should focus on dynamic inflow changes and on the relative performance of wake mixing and wake steering under directional uncertainty. The influence of turbine spacing, inflow characteristic and cluster configuration on how wake mixing could further enhance wake steering remains to be investigated. Moreover, recent studies – such as [17] – have demonstrated the possibility of synchronising wake-mixing actuation on downstream turbines, which could potentially lead to higher power gains.

Acknowledgements

This work has been partially supported by the TWEET-IE project, which receives funding from the European Union's Horizon Europe Programme under the grant agreement No. 101079125. This work has been partially supported by the SUDOCO project, which receives funding from the European Union's Horizon Europe Programme under the grant agreement No. 101122256. This work has been partially supported by the Deutsche Forschungsgemeinschaft (DFG, grant number BR 1511/20-1) under the "WakeAware" project (n. 531570398). The authors express their gratitude to the wind tunnel team at Politecnico di Milano for providing assistance during the experiments.

References

[1] Fleming P A, Gebraad P M, Lee S, van Wingerden J W, Johnson K, Churchfield M, Michalakes J, Spalart P and Moriarty P 2014 Evaluating techniques for redirecting turbine wakes using sowfa *Renewable Energy* **70** 211–218 ISSN 0960-1481 special issue on aerodynamics of offshore wind energy systems and wakes URL `https://www.sciencedirect.com/science/article/pii/S0960148114000950`

[2] Doekemeijer B M, Kern S, Maturu S, Kanev S, Salbert B, Schreiber J, Campagnolo F, Bottasso C L, Schuler S, Wilts F, Neumann T, Potenza G, Calabretta F, Fioretti F and van Wingerden J W 2021 Field experiment for open-loop yaw-based wake steering at a commercial onshore wind farm in italy *Wind Energy Science* **6** 159–176 URL `https://wes.copernicus.org/articles/6/159/2021/`

[3] Taschner E, Becker M, Verzijlbergh R and van Wingerden J 2024 Comparison of helix and wake steering control for varying turbine spacing and wind direction *Journal of Physics: Conference Series* **2767** 032023 URL `https://dx.doi.org/10.1088/1742-6596/2767/3/032023`

[4] Frederik J A, Doekemeijer B M, Mulders S P and van Wingerden J W 2020 The helix approach: Using dynamic individual pitch control to enhance wake mixing in wind farms *Wind Energy* **23** 1739–1751 URL `https://onlinelibrary.wiley.com/doi/abs/10.1002/we.2513`

[5] Gutknecht J, Taschner E, Coquelet M, Viré A and van Wingerden J W 2025 The impact of coherent large-scale vortices generated by helix active wake control on the recovery process of wind turbine wakes *Physics of Fluids* **37** 067162 ISSN 1070-6631 URL `https://doi.org/10.1063/5.0278687`

[6] Munters W and Meyers J 2018 Dynamic strategies for yaw and induction control of wind farms based on large-eddy simulation and optimization *Energies* **11** 177

[7] Lin M and Porté-Agel F 2024 Wake meandering of wind turbines under dynamic yaw control and impacts on power and fatigue *Renewable Energy* **223** 120003 ISSN 0960-1481 URL https://www.sciencedirect.com/science/article/pii/S0960148124000685

[8] Wang C, Campagnolo F, Canet H, Barreiro D J and Bottasso C L 2021 How realistic are the wakes of scaled wind turbine models? *Wind Energy Science* **6** 961–981 URL https://wes.copernicus.org/articles/6/961/2021/

[9] Bottasso C L, Campagnolo F and Petrović V 2014 Wind tunnel testing of scaled wind turbine models: Beyond aerodynamics *Journal of Wind Engineering and Industrial Aerodynamics* **127** 11–28 ISSN 0167-6105 URL https://www.sciencedirect.com/science/article/pii/S0167610514000269

[10] Mühle F V, Campagnolo F, Llobell Buigues J and Bottasso C L 2022 Design and testing of a model-scale yaw mechanism for an experimental wind turbine model *Journal of Physics: Conference Series* **2265** 022094 URL https://doi.org/10.1088/1742-6596/2265/2/022094

[11] Bossanyi E A 2000 The design of closed loop controllers for wind turbines *Wind Energy* **3** 149–163 URL https://onlinelibrary.wiley.com/doi/abs/10.1002/we.34

[12] Taschner E, Vondelen A, Verzijlbergh R and Wingerden J 2023 On the performance of the helix wind farm control approach in the conventionally neutral atmospheric boundary layer *Journal of Physics: Conference Series* **2505** 012006

[13] Campagnolo F, Weber R, Schreiber J and Bottasso C L 2020 Wind tunnel testing of wake steering with dynamic wind direction changes *Wind Energy Science* **5** 1273–1295 URL https://wes.copernicus.org/articles/5/1273/2020/

[14] Korb H, Asmuth H, Stender M and Ivanell S 2021 Exploring the application of reinforcement learning to wind farm control *Journal of Physics: Conference Series* **1934** 012022 URL https://doi.org/10.1088/1742-6596/1934/1/012022

[15] van der Hoek D, den Abbeele B V, Simao Ferreira C and van Wingerden J W 2024 Maximizing wind farm power output with the helix approach: Experimental validation and wake analysis using tomographic particle image velocimetry *Wind Energy* **27** 463–482 (*Preprint* https://onlinelibrary.wiley.com/doi/pdf/10.1002/we.2896) URL https://onlinelibrary.wiley.com/doi/abs/10.1002/we.2896

[16] Thedin R, Barter G, Jonkman J, Mudafort R, Bay C J, Shaler K and Kreeft J 2025 Load assessment of a wind farm considering negative and positive yaw misalignment for wake steering *Wind Energy Science* **10** 1033–1053 URL https://wes.copernicus.org/articles/10/1033/2025/

[17] van Vondelen A A, Ottenheym J, Pamososuryo A K, Navalkar S T and van Wingerden J W 2023 Phase synchronization for helix enhanced wake mixing in downstream wind turbines *IFAC-PapersOnLine* **56** 8426–8431 ISSN 2405-8963 22nd IFAC World Congress URL https://www.sciencedirect.com/science/article/pii/S2405896323014416